Title

Ambient-Pressure Relithiation of Degraded LixNi0.5Co0.2Mn0.3O2 (0 < x < 1) via Eutectic Solutions for Direct Regeneration of Lithium-Ion Battery Cathodes

Journal

Advanced Energy Materials, 9(20)

ISSN

1614-6832

Authors

Shi, Yang
Zhang, Minghao
Meng, Ying Shirley
et al.

Publication Date

2019-05-01

DOI

10.1002/aenm.201900454

Peer reviewed

ADVANCED ENERGY MATERIALS

www.advenergymat.de

Ambient-Pressure Relithiation of Degraded $Li_xNi_{0.5}Co_{0.2}Mn_{0.3}O_2$ ($0 < x < 1$) via Eutectic Solutions for Direct Regeneration of Lithium-Ion Battery Cathodes

*Yang Shi, Minghao Zhang, Ying Shirley Meng, and Zheng Chen**

With the rapid growth of the lithium-ion battery (LIBs) market, recycling and re-use of end-of-life LIBs to reclaim lithium (Li) and transition metal (TM) resources (e.g., Co, Ni), as well as eliminating pollution from disposal of waste batteries, has become an urgent task. Here, for the first time the ambient-pressure relithiation of degraded $LiNi_{0.5}Co_{0.2}Mn_{0.3}O_2$ (NCM523) cathodes via eutectic Li^+ molten-salt solutions is successfully demonstrated. Combining such a low-temperature relithiation process with a well-designed thermal annealing step, NCM523 cathode particles with significant Li loss (≈40%) and capacity degradation (≈50%) can be successfully regenerated to achieve their original composition and crystal structures, leading to effective recovery of their capacity, cycling stability, and rate capability to the levels of the pristine materials. Advanced characterization tools including atomic resolution electron microscopy imaging and electron energy loss spectroscopy are combined to demonstrate that NCM523's original layered crystal structure is recovered. For the first time, it is shown that layer-to-rock salt phase change on the surfaces and subsurfaces of the cathode materials can be reversed if lithium can be incorporated back to the material. The result suggests the great promise of using eutectic Li^+ molten–salt solutions for ambient-pressure relithiation to recycle and remanufacture degraded LIB cathode materials.

Today's lithium-ion batteries (LIBs) can offer high energy density (260 Wh kg^{-1} and 700 Wh L^{-1} at cell level), and high Coulombic efficiency (99.98%) and long cycling life (>1000 cycles), making them the dominating power sources for portable electronics and electric vehicles (EVs).[1,2] Due to rapid growth of their markets, the worldwide manufacturing capacity of LIBs is expected to have a expansion reaching hundreds of GWh per year in the next 5 years.[3] In this context, recycling and re-use of end-of-life LIBs (after 5–10 years of operation) to reclaim lithium (Li) and transition metal (TM) resources (e.g., Co, Ni), as well as eliminating pollution from disposal of waste batteries, has become an urgent task.[4–6]

Great effort has been made to recycling of LIB cathode materials due to the fact that majority of the battery value is embedded in the cathode materials,[7,8] even though it is the ultimate goal to fully recycle every component in the used batteries.[9,10] The state-of-the-art approaches to recycle cathode materials include pyrometallurgy, hydrometallurgy, and direct recycling.[11] The pyrometallurgical approach requires high temperature smelting as well as multistep purification and separation processes; and the hydrometallurgical approach requires acid leaching and subsequent complicated precipitation steps to produce precursors for the re-synthesis of new cathode materials. Both approaches have to totally destruct the LIB cathode particles (e.g., well-tuned secondary particle structures), which represents a significant amount of value due to the embedded energy from their primary manufacturing process. Different from the above methods, direct recycling approach combines a physical separation process to harvest the cathode materials with a posttreatment (e.g., relithiation, annealing) process to heal the compositional and structural defects of the electrode particles, which leads to regenerated cathodes that can be readily used for making new cells. With appropriate conditions, directly regenerated cathode materials may exhibit high specific capacity, high cycling stability, and high rate capability reaching pristine materials but with significantly reduced cost.[12,13] However, relithiation of degraded Li-deficient cathode particles often requires high-temperature and/or high pressure operation to achieve a stoichiometric ratio of Li in the cathode.

$LiNi_{0.5}Co_{0.2}Mn_{0.3}O_2$ (NCM523) is one of the predominant cathode materials in the state-of-the-art LIBs due to its relatively high energy density and low cost (compared with $LiCoO_2$ and $LiNi_{1/3}Co_{1/3}Mn_{1/3}O_2$), as well as its balance in the property

Dr. Y. Shi, Dr. M. Zhang, Prof. Y. S. Meng, Prof. Z. Chen
Department of NanoEngineering
University of California San Diego
La Jolla, CA 92093, USA
E-mail: zhengchen@eng.ucsd.edu
Prof. Y. S. Meng, Prof. Z. Chen
Sustainable Power & Energy Center (SPEC)
University of California San Diego
La Jolla, CA 92093, USA
Prof. Z. Chen
Program of Chemical Engineering
University of California San Diego
La Jolla, CA 92093, USA
The ORCID identification number(s) for the author(s) of this article can be found under https://doi.org/10.1002/aenm.201900454.

DOI: 10.1002/aenm.201900454

matrix including cycling performance, rate capacity, and thermal stability.[14] It is commonly recognized that Li loss is one of the major issues that are responsible for capacity degradation of NCM-based cathodes.[15–17] As Li losses, the TM cations (e.g., Ni^{2+}) start to migrate between the layers, which slowly induces unfavorable phase changes. Since Ni^{2+} and Li^{+} have similar sizes, a higher Ni concentration in the NMC cathode will likely to result in more severe irreversible structure change.[18,19] Accordingly, it poses greater challenge to directly regenerate and recover the electrochemical properties of degraded cathodes with higher Ni contents, such as NCM523. In our previous work, we integrated a hydrothermal relithiation process with a short annealing step to fully resolve the compositional and structural defects in degraded NCM cathodes, which led to successful recovery of the original stoichiometric composition, layered structure, and electrochemical performance of pristine NCM523 cathodes.[13] While the process is relatively simple, high-pressure hydrothermal reaction (220 °C and 10 MPa) is required and additional cost may be incurred to mitigate potential safety concerns. Therefore, it is of great interest to develop a safer, scalable, low-cost, and environment-friendly approach to regenerate degraded NCM cathode materials.

Eutectic molten salt mixture is a class of homogenous system that melts or solidifies at a temperature (eutectic temperature) that is lower than the melting point of any constituent salt at normal pressure.[20] They are found to be useful as "solvents" or precursors for many applications such as thermal energy storage and "solvent-free" chemical reactions.[21–23] Particularly, Li-based eutectic molten salts have been used as both the Li source and the "solvent" to react with TM precursors for the synthesis of high-performance LIB cathodes.[24,25] Among different eutectic systems formed by common Li salts, the mixture of $LiNO_3$ and LiOH at a molar ratio of 3:2 is of great interest for us due to its lowest melting point at ≈175 °C.[26] This type of unique eutectic Li solution system has great potential for relithiation of degraded cathode materials at ambient pressure and low temperature.

In this study, for the first time we attempted ambient-pressure relithiation of degraded Li-deficient NCM523 particles via eutectic Li solutions. We combined an ambient-pressure, low-temperature molten-salt reaction with a short-time thermal annealing to directly regenerate NCM523 cathode particles. We selected commercial LIBs with NCM523 cathodes and investigated the electrochemical performance of the cathodes at three key stages: pristine (beginning-of-life), degraded (end-of-life) and regenerated conditions. By starting from the pristine cathode materials and cycling them to induce significant capacity degradation (≈50%), the whole electrochemical history can be obtained for a reliable evaluation of the recycling and regeneration process. Systematic characterization suggests that the chemical composition (e.g., Li content) and bulk crystal structures can be recovered from this regeneration process. Moreover, the surface rock salt phase (NiO-like) that is formed due to long-term cycling can be also converted to the original layered phase, accompanied by the changes in oxidation states of TMs. With the successful revival of their composition and structure, the Li storage capacity, cycling stability, and rate capability of the degraded NCM523 cathode particles can be recovered to the original levels of the pristine materials, suggesting the promise of using this new method to recycle and remanufacture degraded LIB cathodes. In addition, this work may also provide a unique platform to further study reversible chemistry in various solid-state ionic materials.

It is commonly considered that a LIB cell approaches the end of its life once more than 20% of capacity loss is reached.[27–30] Secondary use of such degraded batteries is possible for maximizing the value of cells since a considerable amount of capacity may remain useful for other purposes such as back-up power sources. However, in order to demonstrate the effectiveness and robustness of our cathode regeneration process, here we intentionally induced more than 20% of capacity degradation. In our experiment, commercial pouch cells with NCM523 cathodes were cycled in the voltage range of 3–4.5 V at 1 C for 400 cycles to achieve a capacity degradation of 48% (Figure S1, Supporting Information). Correspondingly, significant Li^{+} loss (40%) was identified in cathode materials after cycling, as revealed by inductively coupled plasma optical emission spectrometer (ICP-OES). To regenerate the degraded cathode materials and revitalize their electrochemical activity, we need to resolve both the composition (e.g., Li^{+} loss) and structure defects (e.g., phase changes) resulting from long-term cycling.[12,13,31,32] While our previous work on hydrothermal relithiation can successfully reach stoichiometric composition,[12,13] such a relithiation process brings up concerns for large-scale operation due to the required high pressure. To mitigate this potential issue, it is desirable to develop an ambient-pressure relithiation strategy.

Our approach aimed to restore the Li composition in degraded NCM cathodes via an eutectic Li-molten salt solution at ambient pressure. Li-molten salt solutions based on different Li salts have been explored for electrolytes in LIBs or lithium oxygen batteries.[33–35] Among these solutions, Li–salt mixtures of $LiNO_3$ and LiOH can form a wide range of eutectic solutions. Especially, when it is composed of LiOH and $LiNO_3$ at a molar ratio of 2:3, its melting point reaches as low as 176 °C, as displayed in their phase diagram (**Figure 1**a). Therefore, such a ratio was adopted in the preparation of eutectic molten salt solutions for relithiation of degraded NCM523 cathodes at ambient pressure.

Our hypothesis is that the eutectic solution with high Li^{+} concentration can effectively relithiate the Li-deficient LIB cathodes without using any extra pressure. As illustrated in Figure 1b, degraded NMC523 particles with Li vacancies are mixed with $LiNO_3$ and LiOH at a molar ratio of 3:2. The mixture is then heated to 300 °C at ambient pressure and held for 2–4 h to allow sufficient time for Li^{+} diffusion through the particles, which results in complete relithiation of the Li-deficient cathode particles.

Thermal analysis was first carried out to elucidate the relithiation process of the degraded NCM523 in the eutectic Li molten-salt solution and to determine the appropriate reaction temperature. Differential scanning calorimetry (DSC) analysis was performed on the mixture of degraded particles and eutectic Li salts (**Figure 2**a). The endothermic peak at 100 °C corresponds to the loss of absorbed water from $LiNO_3$ since it is hygroscopic, as revealed in the dramatic weight loss in the thermogravimetric analysis (TGA) curve (Figure 2b). A second endothermic peak at 176 °C corresponds to the melting of the eutectic molten salt.[26] The exothermic peak at 250 °C

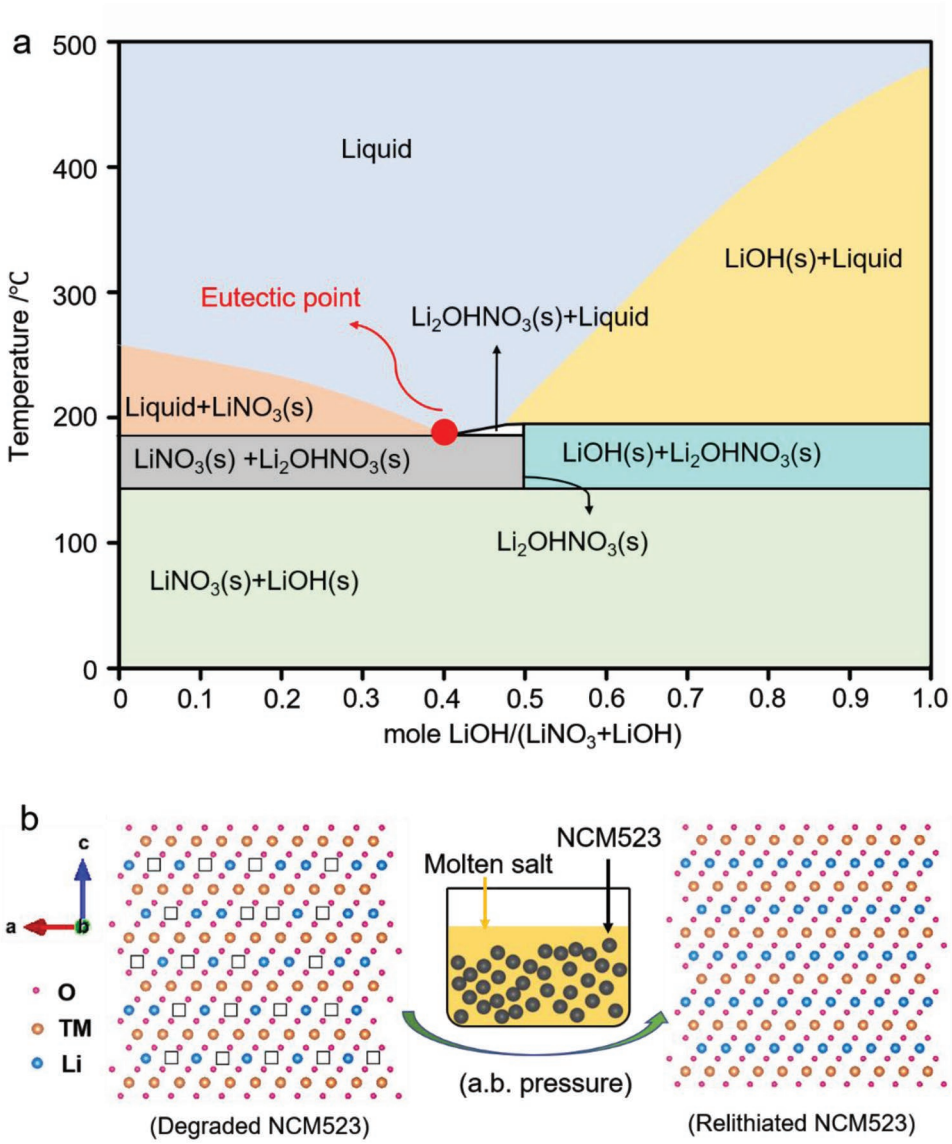

Figure 1. a) Phase diagram of $LiNO_3$ and LiOH (reproduced from FACT salt database).[36] b) Illustration of the relithiation process for Li composition recovery via the eutectic molten salt approach (a.b.: ambient).

(Figure 2a) and the corresponding weight loss in the temperature range of 250–350 °C can be ascribed to gas evolution. Possible reactions in this temperature ranges include the lithiation of the degraded cathode materials associated with the generation of O_2, water (vapor), and NO_2:

$$Li_{1-x}Ni_{0.5}Co_{0.2}Mn_{0.3}O_2 + xLiOH \rightarrow LiNi_{0.5}Co_{0.2}Mn_{0.3}O_2 + \frac{x}{2}H_2O + \frac{x}{4}O_2 \quad (1)$$

$$Li_{1-x}Ni_{0.5}Co_{0.2}Mn_{0.3}O_2 + xLiNO_3 \rightarrow LiNi_{0.5}Co_{0.2}Mn_{0.3}O_2 + xNO_2 + \frac{x}{2}O_2 \quad (2)$$

No obvious endothermic or exothermic peaks are observed upon only heating degraded NCM523, though a broad exothermic peak between 300 °C and 400 °C is observed (Figure 2b), which is due to the oxygen loss of Li-deficient NCM cathode.[37] This result suggests that the lithiation reaction of degraded NCM523 with the eutectic Li-molten salts mainly occurs at ≈250 °C, therefore a temperature of 300 °C is selected for the relithiation experiment.

With full relithiation, thermal annealing was then performed to promote the crystallization of the particles to form desired layered phase. After complete regeneration, the chemical compositions of the pristine, degraded and regenerated NCM523 cathode materials were determined and compared (**Table 1**). The materials only underwent relithiation with molten salts for 2 and 4 h are denoted as "MS-2 h" and "MS-4 h," respectively. The samples with relithiation and short annealing are denoted as "MS-SA 2 h" and "MS-SA 4 h," respectively. The degraded NCM523 material had a Li loss of ≈40%, which further

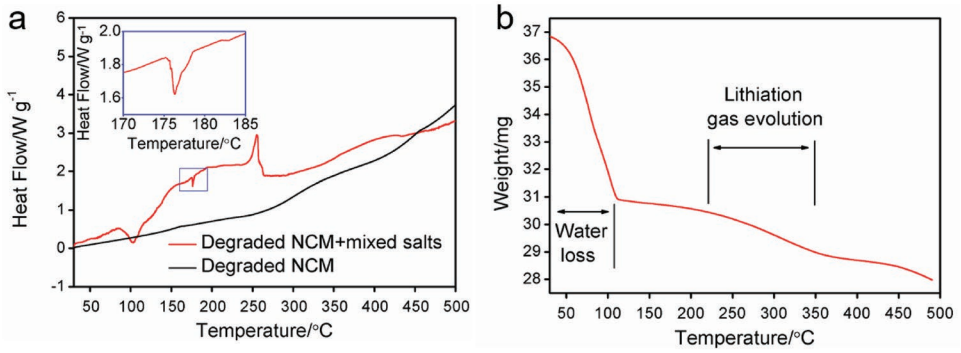

Figure 2. a) DSC curves of degraded NCM523 particles and the mixture of degraded NCM523 particles and the eutectic Li-salt ($LiOH:LiNO_3$ = 2:3 in mole). b) TGA curve of the mixture of degraded NCM523 particles and the eutectic Li–salt.

confirms that Li loss is the main cause responsible for its capacity loss (48%). While it is very close to the stoichiometric ratio, the Li content of the MS-2 h sample is slightly lower than that of the pristine NCM523 sample, indicating that a longer time is needed to overcome the lithiation kinetics. With 4 h of relithiation with the Li-molten salts (MS-4 h), the Li concentration of the degraded NCM523 particles can be fully recovered to the pristine composition. Note that doubling the relithiation time only led to limited overdosage of Li (1.7%). This result indicates that the relithiation in the eutectic Li salt is a self-saturation process, which agrees with the kinetics observed in the hydrothermal relithiation process.[13] Although the Li^+ content can be fully recovered by the lithiation step, a short annealing step is also critical to reach the desired crystallinity. In our previous work on the regeneration of $LiCoO_2$ cathodes through a hydrothermal lithiation process, their Li^+ content can be completely recovered but the lithiated sample still shows poor cycling performance without annealing due to the existence of phase impurities.[12] We also identified that without an annealing step, degraded NCM523 with hydrothermal lithiation presented a significant amount of amorphous domains on the surface of their particles.[13] Therefore, the short-annealing step is required to recover the electrochemical performance and crystal structure of degraded cathodes. Since 5% of extra Li was added to compensate the Li evaporation during the annealing step, both MS-SA 2 h and MS-SA 4 h reached saturated Li ratio with slight overdosage, which is close to the composition in the pristine NCM523 sample.

The X-ray powder diffraction (XRD) patterns of the pristine, cycled (degraded) and regenerated NCM523 particles are shown in **Figure 3**. All the samples exhibit a typical pattern of α-$NaFeO_2$ structure with $R\bar{3}m$ space group. The degraded particles showed a larger intensity ratio of I_{003}/I_{104} compared with the pristine sample, which is consistent with some previous report.[32,38] For example, in the work of Jung et al., the cycled NCM523 cathode showed higher I_{003}/I_{104} ratio.[32] Additionally, Weigel et al. also showed that some of the cycled NCM811 cathode samples also had higher I_{003}/I_{104} ratio and lower cation mixing.[38] The reason for this phenomenon might be related to the preferred orientation of certain facets after microstructure changes during cycling.[39,40] The (003) peak shifted to lower angles, corresponding to an increase in *c* lattice parameter due to the electrostatic repulsion between the oxygen layers along *c* directions in the Li-deficient state.[41] The spacing between the peaks in the (108)/(110) doublets increased after cycling, corresponding to the decrease in *a* lattice parameters due to the smaller effective ionic radii of Ni^{3+} than Ni^{2+} to compensate Li deficiency.[42] The merging of (006)/(102) doublets indicates the feature of spinel phase. It is well known that the transition from layered to spinel phase can occur during charge/discharge cycling, especially on the surface of the cathode particles, due to the migration of TMs to the Li sites.[32] After extensive cycling and serious degradation of the cathodes, the spinel phase spreads from the surface to the bulk regions, which can be detected in XRD patterns. After regeneration, the shifting of (003) peak toward higher angles, the decrease of spacing between the 108/110 doublets peaks, and the appearance of the separate (006)/(102) doublets together indicate the recovery of the layered crystal structure. Rietveld refinement using structural model was performed on all the XRD patterns to provide quantitative structure information (Figure S2, Supporting Information), and the lattice parameters are compared in **Table 2**. The refinement results further confirm that the degraded particles have decreased *a* lattice parameters and increased *c* lattice parameters. The Li/Ni mixing in the degraded material was calculated to be lower (1.35%) than the pristine material (3.39%). The value of the cycled material may not reflect the real degree of cation mixing due to the possible preferred orientation of NCM523 after cycling. It is a fair comparison of cation mixing in pristine materials (as-synthesized and before cycling), while the cation mixing in cycled materials needs further investigation and is be an important topic for future investigation. For all the regeneration conditions, the *a* and *c* lattice parameters

Table 1. ICP-OES results of pristine, cycled and regenerated NCM523 cathode particles.

Sample	Composition
Pristine	$Li_{1.009}Ni_{0.492}Co_{0.209}Mn_{0.305}O_{2.015}$
Degraded	$Li_{0.593}Ni_{0.491}Co_{0.202}Mn_{0.301}O_{2.005}$
MS-2 h	$Li_{0.995}Ni_{0.491}Co_{0.209}Mn_{0.302}O_{2.010}$
MS-4 h	$Li_{1.011}Ni_{0.491}Co_{0.208}Mn_{0.304}O_{2.009}$
MS-SA 2 h	$Li_{1.002}Ni_{0.490}Co_{0.210}Mn_{0.302}O_{2.011}$
MS-SA 4 h	$Li_{1.019}Ni_{0.492}Co_{0.209}Mn_{0.303}O_{2.012}$

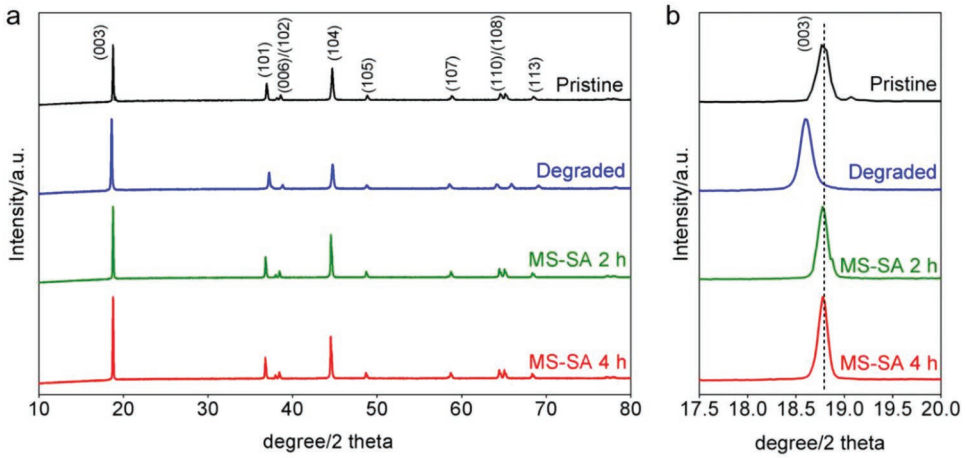

Figure 3. XRD patterns of pristine, degraded and regenerated NCM523 particles, a) 10–80°, b) 17.5–20°.

change back to higher and lower values, respectively, suggesting the recovery of the crystal structure. The Li/Ni mixing of MS-SA 4 h sample is lower than that of MS-SA 2 h sample, which is resulted from the longer lithiation time of the former sample, since increased Li content can suppress the cation mixing.[43,44]

The microphase changes of degraded (**Figure 4**a) and regenerated (Figure 4b) samples were carefully examined by high-resolution transmission electron microscopy (HRTEM). MS-SA 4 h sample was selected as the representative regenerated sample for the microscopic characterization due to its lower cation mixing. More than 10 particles were examined for each sample. Figure 4 shows the data of representative particles. The degraded NCM523 particles clearly showed rock salt phase existed near the surface region (Figure 4c) and layered phase in the bulk region (Figure 4d). The characteristic spots in FFT pattern of rock salt phase can be indexed as $(1\bar{1}1)$, (002) and $(\bar{1}11)$ plane in the zone axis of [110]. As expected, the intensity profile exhibits periodic contrast along the TM layer from the surface to the bulk in both the degraded sample (Figure 4h) and regenerated sample (Figure 4j) with a nearest atomic column distance ≈0.28 nm. However, the intensity profile of the degraded sample along the Li layer shows much higher intensity on the surface, which indicates the presence of a blocking layer due to the existence of TM at the Li layer (Figure 4g). It has been demonstrated that the migration of TM to the Li layer during cycling can block the Li^+ transport, resulting in capacity degradation.[32,45,46] After regeneration (Figure 4b), only the layered phase was observed on the surface (Figure 4e) and in the bulk (Figure 4f). Consistently, the intensity profile along the Li layer exhibits uniform contrast both on the surface and in the bulk (Figure 4i), which proves that the rock–salt phase was eliminated after regeneration and the layered phase was successfully recovered.

Table 2. Lattice parameters of pristine, cycled and regenerated cathode particles.

Sample	*a* [Å]	*c* [Å]	Li/Ni mixing	R_B	R_{wp}
Pristine	2.8689(4)	14.240(6)	3.39%	4.41%	1.65%
Degraded	2.8397(1)	14.423(1)	1.35%	6.28%	2.06%
MS-SA 2 h	2.8674(8)	14.232(4)	3.62%	6.31%	1.83%
MS-SA 4 h	2.8680(0)	14.231(3)	2.43%	5.41%	1.86%

To exam the oxidation state of the TM ions on the surface and in the bulk, electron energy loss spectroscopy (EELS) was performed on the degraded (**Figure 5**a) and regenerated (Figure 5b) samples, with the cross symbol (×) indicating the positions of measurement. Note that all the EELS spectra were normalized to Ni M-edge in the low-loss region and O K-edge in the high-loss region. A comparison of the Li K-edge spectra in the bulk of degraded and regenerated NCM523 samples shows a much higher Li content after regeneration (Figure 5c), which is consistent with the ICP-OES results. The broad structures of O K-edge above 534 eV correspond to the transition of O 1s to the hybridized states, consisting of TM 4sp and oxygen 2p orbitals. The pre-edge structure below 534 eV corresponds to the transition to the states of TM 3d and oxygen 2p orbitals. The intensity ratio of the 3d to 4sp band represents the amount of unoccupied 3d orbitals in the TM ions and a change in the local environment of oxygen.[47] The decrease of pre-edge structure of the degraded sample suggests the change of bond covalency between oxygen and the neighboring TM, which is due to the formation of Ni–O like rock-salt structure on the surface of the material.

In the regenerated sample, no obvious difference of pre-edge structure was observed from the surface to the bulk, which once again manifests the surface structure recovery (Figure 5d).[48,49] The differences in the Mn L-edge spectra of degraded and regenerated samples are also obvious (Figure 5e). In the degraded sample, the red shift of the absolute energy onset on the surface compared to the bulk together with a higher L_3/L_2 ratio on the surface than that in the bulk suggests a lower oxidation state of Mn on the surface due to the surface oxygen loss during cycling.[50] The regenerated sample shows similar Mn L-edge peaks on the surface and in the bulk, which suggests that the oxidation state of Mn is identical from the surface to the bulk after regeneration. The oxidation states of Co are similar on both the surface and in the bulk, as well as in degraded and regenerated samples, which is evidenced from similar peak positions and intensities of Co L-edge spectra in all the samples (Figure 5f). In Ni L-edge spectra (Figure 5g), the regenerated sample shows lower oxidation state than the

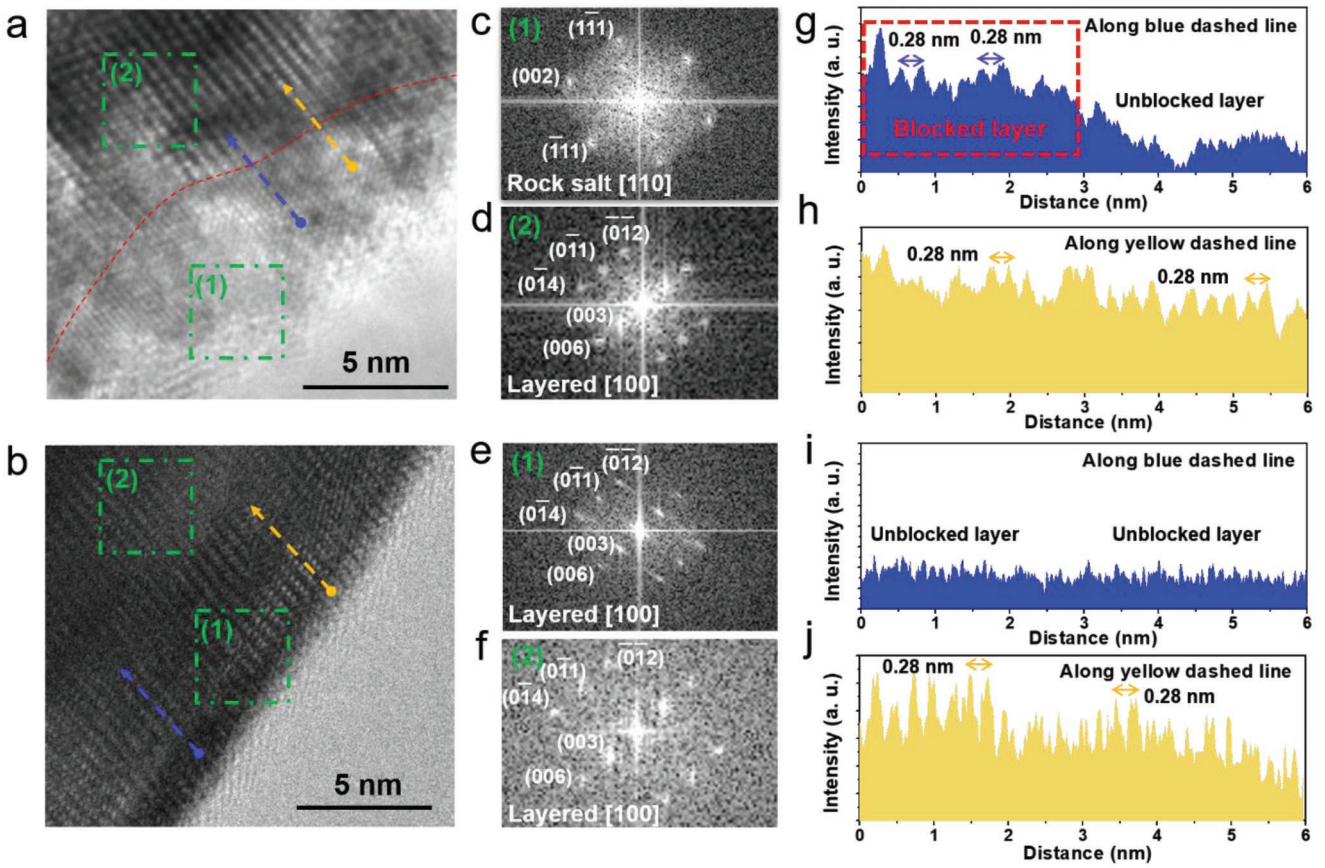

Figure 4. a,b) HRTEM images of degraded and regenerated NCM523 particles. c–f) FFT from the region indicated by green dashed rectangle in (a) and (b), respectively. g,i) Intensity plot along the blue dashed line shown in (a,b). h,j) Intensity plot along the yellow dashed line shown in (a,b).

degraded sample, which is attributed to the charge compensation due to re-dosed Li after regeneration. To investigate whether the regeneration process changed the TM distributions, scanning transmission electron microscopy-energy dispersive X-ray spectroscopy (STEM/EDS) mapping were performed on the degraded (Figure S3, Supporting Information) and regenerated (Figure S4, Supporting Information) samples. Both the degraded and regenerated samples showed similarly uniform TM distribution, suggesting that the regeneration procedure has neglectable contribution to the TM distribution.

The charge/discharge cycling performance of the pristine and regenerated NCM523 cathode particles was evaluated in a voltage range of 3–4.3 V at 1 C (C = 150 mA g^{-1}) after one activation cycle at C/10 (**Figure 6**a) and their voltage profiles at different cycles are compared (Figure 6b). The pristine cathode shows a capacity of 146.6 mAh g^{-1} in the first cycle at 1 C and 130.4 mAh g^{-1} after 100 cycles (Figure 6a). Although the original graphite/NCM523 pouch cells were cycled to induce ≈48% of capacity degradation with 40% of Li^+ loss in the cathodes, the electrochemical activity and cycling stability of the regenerated NCM523 cathodes can be fully recovered: the MS-SA 4 h sample shows a capacity of 149.3 mAh g^{-1} in the first cycle at 1 C and 134.6 mAh g^{-1} after 100 cycles. This performance is even slightly better than the original NCM523 sample, possibly due to the reduced cation mixing the in bulk of the cathode particles after uniform relithiation. The MS-SA 2 h sample has inferior cycling stability and large voltage drop at the beginning of discharge cycles (Figure 6b), which is due to its higher Li/Ni cation mixing: the higher charge of Ni^{2+} can lead to a stronger electrostatic repulsion of the migrating of Li^+,[44] and disordered Li slab are more contracted in distance, making Li^+ diffusion more difficult.[51] The MS-SA 4 h sample shows good rate capability, similar with that of the pristine sample, while the MS-SA 2 h sample has inferior rate capability (Figure 6c,d). For example, MS-SA 4 h sample has a discharge capacity of 124.4 mAh g^{-1} at 5 C, while MS-SA 2 h sample only has a capacity of 108.4 mAh g^{-1} at 5 C. The better rate performance of the MS-SA 4 h sample is attributed to its lower Li^+ migration barrier.

In summary, for the first time we successfully demonstrated ambient-pressure relithiation of degraded, lithium-deficient NCM523 particles via a eutectic Li^+ molten–salt solutions. By combining such a low-temperature molten–salt relithiation process with a short-time thermal annealing step, NCM523 cathode particles with significant capacity degradation and Li loss can be successfully regenerated to achieve their original chemical composition and crystal structures. As a result, the Li storage capacity, cycling stability, and rate capability of the degraded cathodes can be recovered to the original levels of the pristine materials, suggesting the promise of using this new method to recycle and remanufacture degraded NCM cathode materials. We believe that this method can be extended

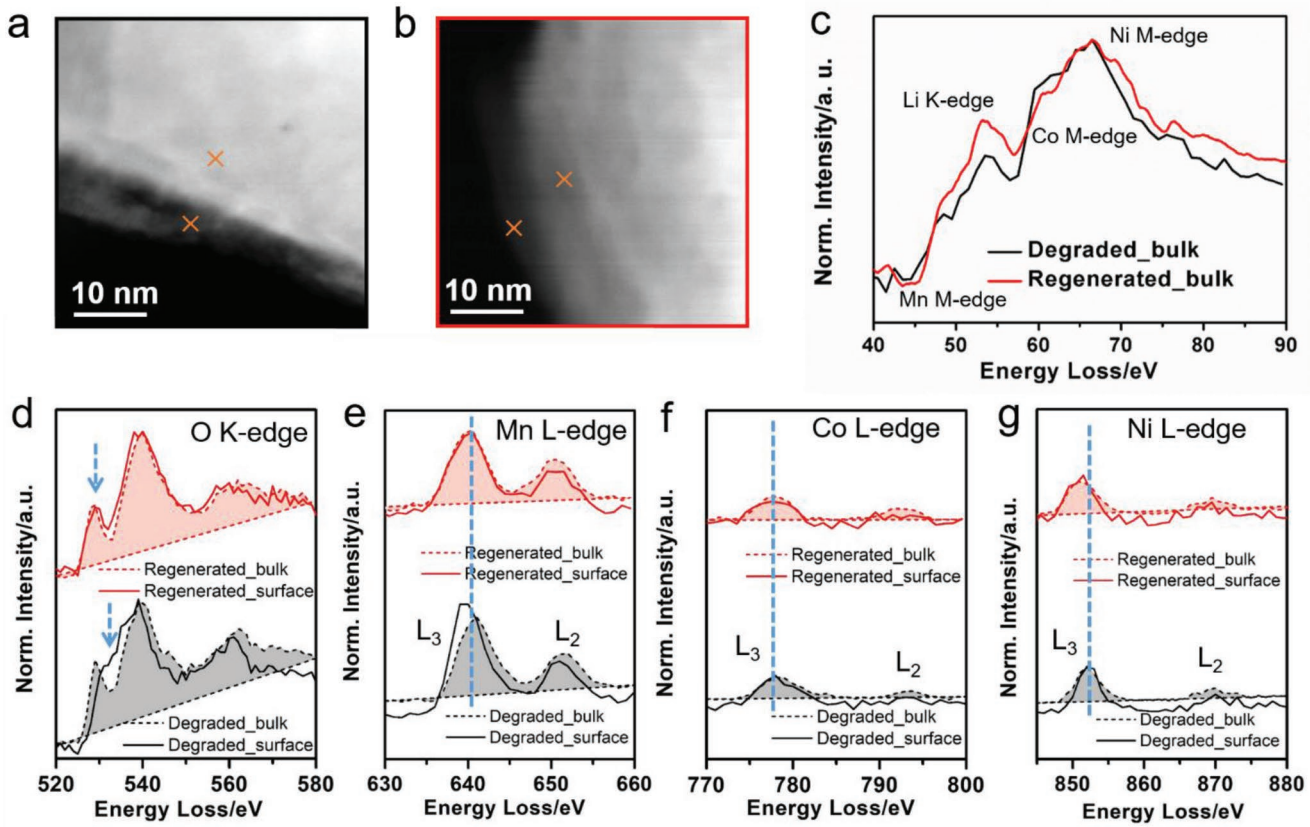

Figure 5. a,b) STEM images of degraded and regenerated NCM523 particles. c) Low-loss region of EELS for the bulk of particles. d–g) EELS comparison of the surface and bulk in the degraded and regenerated sample for O K-edge, Mn L-edge, Co L-edge, and Ni L-edge, respectively.

and applied to regenerate other LIB cathode materials such as $LiMn_2O_4$, $LiFePO_4$ as well as sodium-ion battery cathodes (e.g., $Na(Ni_{0.60}Co_{0.05}Mn_{0.35})O_2$), though the exact details of the treatment may vary depending on the cathode structures and chemistries. In addition, this work may also provide a unique platform to further study reversible chemistry in various solid-state ionic materials to develop green synthetic strategies for energy materials.

Experimental Section

Pouch Cells Assembly and Cathode Materials Harvesting: Dry pouch cells (220 mAh) with NCM523 as the cathode and graphite as the anode were purchased from Li-Fun Technology (Xinma Industry Zone, Golden Dragon Road, Tianyuan District, Zhuzhou City, Hunan Province, PRC, 412 000). Electrolyte was filled in and the pouch cell was sealed by a vacuum sealer (MTI corporation) in an argon-filled glovebox. The electrolyte (LP40) was 1 M $LiPF_6$ in ethylene carbonate (EC) and diethyl carbonate (DEC) with a weight ratio of 1:1. After formation at *C*/10 (*C* = 150 mA g^{-1}) for the first cycle, the pouch cells were cycled in the voltage range of 3–4.5 V at 1 C for 400 cycles to induce capacity decay. All pouch cells were discharged to 2 V at *C*/10 before disassembly.

To harvest NCM523 cathode particles, the cathode strips were harvested from the pouch cell, thoroughly rinsed by dimethyl carbonate and soaked in N-methyl-2-pyrrolidone (NMP) followed by sonication. The active materials, binder and carbon black (CB) were removed from the aluminum substrate. The suspension was centrifuged and the active materials were precipitated. The precipitation was washed several times and the active materials were harvested and dried. CB has much lower density than NCM523 and can be separated by gravity during the precipitation process.

Regeneration of Cathode Materials: Degraded NCM523 materials were mixed with an excess amount of a eutectic Li salt mixture which was composed of $LiNO_3$ and LiOH in a molar ratio of 3:2. The mixture was heated at 300 °C for 2 or 4 h for relithiation, and then washed with deionized water to remove the residue Li salts. The relithiated NCM523 was sintered together with 5% excess amount of Li_2CO_3 (to compensate Li loss at high temperature) at 850 °C in oxygen for 4 h. The temperature ramping rate was 5 °C min^{-1}.

Characterization of Materials: The composition of pristine, degraded and regenerated NCM523 cathode was measured by an ICP-OES (Perkin Elmer Optima 3000 DV). DSC analysis of pure degraded NCM523 powder, as well as the mixture of degraded NCM523 and the eutectic Li salts was carried out from room temperature to 500 °C, using a Perkin Elmer Diamond DSC. TGA of the mixture of degraded NCM523 and the eutectic Li salts was performed in the same temperature range with DSC analysis, using Perkin Elmer Pyris 1 TGA. Both DSC and TGA tested were carried out with a temperature ramping rate of 5 °C min^{-1}. The crystal structure of all the cathode powder was examined by XRD employing Cu Kα radiation.

Electrochemical Characterization: To prepared electrodes, the pristine, cycled and regenerated NCM523 cathode materials were mixed with polyvinylidene difluoride (PVDF) binder, and Super P65 at a mass ratio of 8:1:1 in NMP to form slurries. The slurries were cast on aluminum foil using a doctor blade and then dried in vacuum at 80 °C for 6 h. Disc-shape electrodes were cut and compressed by a rolling mill. The active mass loading was about 3 mg cm^{-2}. Type-2016 coin cells were assembled with Li metal disc (thickness: 1.1 mm) as the anode, 1 M $LiPF_6$ in EC: DEC (1:1 wt) as the electrolyte, and trilayer membrane

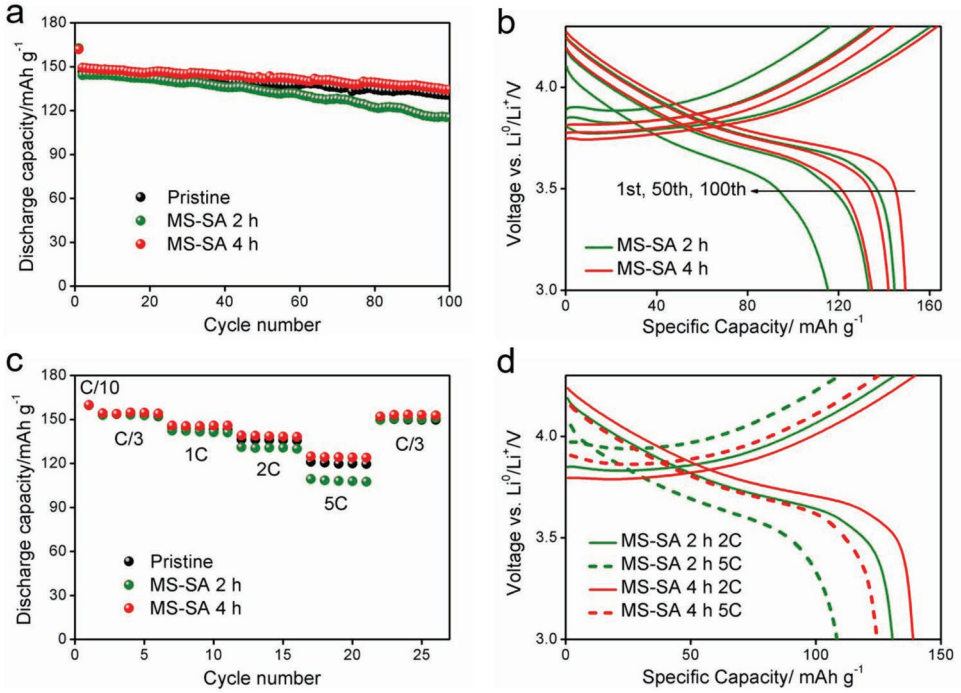

Figure 6. a) Cycling performance of pristine and regenerated cathodes (rate in the initial cycle: *C*/10 ($C = 150$ mA g^{-1}); rate in the following cycles: 1 C). b) Voltage–capacity profiles of regenerated cathodes at different cycles. c) Rate performance of pristine and regenerated cathodes. d) Voltage–capacity profiles of regenerated cathodes at different rates.

(Celgard 2320) as the separator. Galvanostatic charge–discharge was carried out using a LAND battery testing system in the potential range of 3–4.3 V at 1 C after *C*/10 activation in the initial cycle.

Microscopic Characterization: HRTEM was recorded on a field emission gun JEOL-2800 at 200 kV with Gatan OneView Camera (full 4 K * 4 K resolution). STEM-EDS was performed on primary particles using a JEOL JEM-2800 at annular dark field (ADF) mode. All ADF images were acquired at 200 kV with a beam size of ≈5 Å. STEM-EELS was performed on JEOL JEM-ARM300CF at 300 kV, equipped with double correctors. To minimize possible electron beam irradiation effects, EELS spectra were acquired from areas without pre-beam irradiation.

Supporting Information

Supporting Information is available from the Wiley Online Library or from the author.

Acknowledgements

Z.C. gratefully acknowledges funding from US National Science Foundation via Award CBET-1805570, US Department of Energy via ReCell Center, and the start-up fund support from the Jacob School of Engineering at UC San Diego. M.Z. and Y.S.M. acknowledge the funding support from Zable Endowed Chair Fund.

Conflict of Interest

A patent was filed for this work through the UCSD Office of Innovation and Commercialization.

Keywords

cathodes, eutectic solution, lithium-ion batteries, regeneration, relithiation

Received: February 6, 2019
Revised: March 17, 2019
Published online:

[1] T. Placke, R. Kloepsch, S. Dühnen, M. Winter, *J. Solid State Electrochem.* **2017**, *21*, 1939.
[2] P. Meister, H. Jia, J. Li, R. Kloepsch, M. Winter, T. Placke, *Chem. Mater.* **2016**, *28*, 7203.
[3] B. Nykvist, F. Sprei, M. Nilsson, *Energy Policy* **2019**, *124*, 144.
[4] T. C. Wanger, *Conserv. Lett.* **2011**, *4*, 202.
[5] S. Natarajan, V. Aravindan, *Adv. Energy Mater.* **2018**, *8*, 1802303.
[6] X. Zhang, L. Li, E. Fan, Q. Xue, Y. Bian, F. Wu, R. Chen, *Chem. Soc. Rev.* **2018**, *47*, 7239.
[7] A. Kwade, W. Haselrieder, R. Leithoff, A. Modlinger, F. Dietrich, K. Droeder, *Nat. Energy* **2018**, *3*, 290.
[8] G. Berckmans, M. Messagie, J. Smekens, N. Omar, L. Vanhaverbeke, J. Van Mierlo, *Energies* **2017**, *10*, 1314.
[9] W. Lv, Z. Wang, H. Cao, Y. Sun, Y. Zhang, Z. Sun, *ACS Sustainable Chem. Eng.* **2018**, *6*, 1504.
[10] X. Z. Li Li, M. Li, R. Chen, F. Wu, K. Amine, J. Lu, *Electrochem. Energy Rev.* **2018**, *1*, 461.
[11] L. Gaines, *Sustainable Mater. Technol.* **2018**, *17*, e00068.
[12] Y. Shi, G. Chen, Z. Chen, *Green Chem.* **2018**, *20*, 851.
[13] Y. Shi, G. Chen, F. Liu, X. Yue, Z. Chen, *ACS Energy Lett.* **2018**, *3*, 1683.
[14] Y. Shi, M. Zhang, C. Fang, Y. S. Meng, *J. Power Sources* **2018**, *394*, 114.

[15] Q. Zhang, R. E. White, *J. Power Sources* **2008**, *179*, 793.
[16] F. Holtstiege, A. Wilken, M. Winter, T. Placke, *Phys. Chem. Chem. Phys.* **2017**, *19*, 25905.
[17] J. Xu, R. D. Deshpande, J. Pan, Y. T. Cheng, V. S. Battaglia, *J. Electrochem. Soc.* **2015**, *162*, A2026.
[18] Y. Koyama, H. Arai, I. Tanaka, Y. Uchimoto, Z. Ogumi, *Chem. Mater.* **2012**, *24*, 3886.
[19] W. Liu, P. Oh, X. Liu, M. J. Lee, W. Cho, S. Chae, Y. Kim, J. Cho, *Angew. Chem., Int. Ed.* **2015**, *54*, 4440.
[20] M. M. Rahman, J. Z. Wang, M. F. Hassan, S. Chou, D. Wexler, H. K. Liu, *J. Power Sources* **2010**, *195*, 4297.
[21] Z. Yang, S. V. Garimella, *Appl. Energy* **2010**, *87*, 3322.
[22] D. Brosseau, J. W. Kelton, D. Ray, M. Edgar, K. Chisman, B. Emms, *J. Sol. Energy Eng.* **2005**, *127*, 109.
[23] D. Kundu, R. K. Debnath, A. Majee, A. Hajra, *Tetrahedron Lett.* **2009**, *50*, 6998.
[24] L. Wen, Q. Lu, G. X. Xu, *Electrochim. Acta* **2006**, *51*, 4388.
[25] M. V. Reddy, G. V. S. Rao, B. V. R. Chowdari, *J. Power Sources* **2006**, *159*, 263.
[26] Z. R. Chang, X. Yu, H. W. Tang, X. Z. Yuan, H. Wang, *Powder Technol.* **2011**, *207*, 396.
[27] Z. Wang, S. Zeng, J. Guo, T. Qin, *PLoS One* **2018**, *13*, e0200169.
[28] D. Liu, W. Xie, H. Liao, Y. Peng, *IEEE Trans. Instrum. Meas.* **2015**, *64*, 660.
[29] S. J. Harris, D. J. Harris, C. Li, *J. Power Sources* **2017**, *342*, 589.
[30] X. Han, M. Ouyang, L. Lu, J. Li, *Energies* **2014**, *7*, 4895.
[31] R. Hausbrand, G. Cherkashinin, H. Ehrenberg, M. Gröting, K. Albe, C. Hess, W. Jaegermann, *Mater. Sci. Eng., B* **2015**, *192*, 3.
[32] S. K. Jung, H. Gwon, J. Hong, K. Y. Park, D. H. Seo, H. Kim, J. Hyun, W. Yang, K. Kang, *Adv. Energy Mater.* **2014**, *4*, 1300787.
[33] B. Garcia, S. Lavallée, G. Perron, C. Michot, M. Armand, *Electrochim. Acta* **2004**, *49*, 4583.
[34] K. Kubota, H. Matsumoto, *ECS Trans.* **2016**, *73*, 95.
[35] V. Giordani, D. Tozier, H. Tan, C. M. Burke, B. M. Gallant, J. Uddin, J. R. Greer, B. D. McCloskey, G. V. Chase, D. Addison, *J. Am. Chem. Soc.* **2016**, *138*, 2656.
[36] FTsalt-Fact Salt Phase Diagrams, http://www.crct.polymtl.ca/fact/phase_diagram.php?file=LiNO3-LiOH.jpg&dir=FTsalt, (accessed: October 2018).
[37] Y. Shi, M. Zhang, D. Qian, Y. S. Meng, *Electrochim. Acta* **2016**, *203*, 154.
[38] T. Weigel, F. Schipper, E. M. Erickson, F. A. Susai, B. Markovsky, D. Aurbach, *ACS Energy Lett.* **2019**, *4*, 508.
[39] J. B. Bates, N. J. Dudney, B. J. Neudecker, F. X. Hart, H. P. Jun, S. A. Hackney, *J. Electrochem. Soc.* **2000**, *147*, 59.
[40] Y. C. Chen, X. J. Xu, H. Z. Cui, K. H. Dai, Z. S. Song, W. J. Jung, L. Qi, *Acta Phys.-Chim. Sin.* **2007**, *23*, 1948.
[41] D. Mohanty, S. Kalnaus, R. A. Meisner, K. J. Rhodes, J. Li, E. A. Payzant, D. L. Wood, C. Daniel, *J. Power Sources* **2013**, *229*, 239.
[42] D. Mohanty, H. Gabrisch, *J. Power Sources* **2012**, *220*, 405.
[43] F. Wu, J. Tian, Y. Su, J. Wang, C. Zhang, L. Bao, T. He, J. Li, S. Chen, *ACS Appl. Mater. Interfaces* **2015**, *7*, 7702.
[44] F. Schipper, E. M. Erickson, C. Erk, J. Y. Shin, F. F. Chesneau, D. Aurbach, *J. Electrochem. Soc.* **2017**, *164*, A6220.
[45] H. J. Noh, S. Youn, C. S. Yoon, Y. K. Sun, *J. Power Sources* **2013**, *233*, 121.
[46] S. M. Bak, E. Hu, Y. Zhou, X. Yu, S. D. Senanayake, S. J. Cho, K.-B. Kim, K. Y. Chung, X. Q. Yang, K. W. Nam, *ACS Appl. Mater. Interfaces* **2014**, *6*, 22594.
[47] B. Qiu, M. Zhang, L. Wu, J. Wang, Y. Xia, D. Qian, H. Liu, S. Hy, Y. Chen, K. An, Y. Zhu, Z. Liu, Y. S. Meng, *Nat. Commun.* **2016**, *7*, 12108.
[48] F. Lin, I. M. Markus, D. Nordlund, T. C. Weng, M. D. Asta, H. L. Xin, M. M. Doeff, *Nat. Commun.* **2014**, *5*, 3529.
[49] L. Mu, R. Lin, R. Xu, L. Han, S. Xia, D. Sokaras, J. D. Steiner, T. C. Weng, D. Nordlund, M. M. Doeff, Y. Liu, K. Zhao, H. L. Xin, F. Lin, *Nano Lett.* **2018**, *18*, 3241.
[50] J. Graetz, C. C. Ahn, H. Ouyang, P. Rez, B. Fultz, *Phys. Rev. B* **2004**, *69*, 235103.
[51] K. Kang, G. Ceder, *Phys. Rev. B* **2006**, *74*, 094105.